



Title	Determination of appropriate conversion factors for calculating size-specific dose estimates based on X-ray CT scout images after miscentering correction
Author(s)	Terashima, Marin; Mizonobe, Kazufusa; Date, Hiroyuki
Citation	Radiological physics and technology, 12(3), 283-289 https://doi.org/10.1007/s12194-019-00519-5
Issue Date	2019-09
Doc URL	http://hdl.handle.net/2115/79366
Rights	This is a post-peer-review, pre-copyedit version of an article published in Radiological Physics and Technology. The final authenticated version is available online at: http://dx.doi.org/10.1007/s12194-019-00519-5
Type	article (author version)
File Information	RPT_Terashima_Final_2019.6.4.pdf



[Instructions for use](#)

1
2 **Determination of appropriate conversion factors for calculating size-specific dose**
3 **estimates based on X-ray CT scout images after miscentering correction**

4
5 Optimization of size-specific dose estimate through miscentering correction of CT scout images

6
7 Marin Terashima⁽¹⁾, Kazufusa Mizonobe⁽²⁾, Hiroyuki Date⁽³⁾

8 ⁽¹⁾Graduate School of Health Sciences, Hokkaido University

9 e-mail : marinsan.0429@gmail.com

10 ⁽²⁾Division of Radiology and Nuclear medicine, Sapporo Medical University Hospital

11 (Current address : Department of Radiation Oncology, Kobe Minimally invasive Cancer Center)

12 ⁽³⁾Faculty of Health Sciences, Hokkaido University

13
14 **Abstract**

15 In this study, we proposed and evaluated the validity of an optimized size-specific dose estimate, a
16 widely used index of radiation dose in X-ray computed tomography (CT) examinations. Based on
17 miscentering correction of scout images, we determined the appropriate conversion factors (CF) by
18 using a phantom. Scans were conducted using a multi-detector CT system (Aquilion ONE, Canon
19 Medical Systems). Four cylindrical phantoms were taken in the anteroposterior (AP) and axial
20 directions to determine the relationship between pixel value and water-equivalent length (L_w). In the
21 AP scout image, the pixel values at the selected slice positions were converted to L_w to calculate the
22 water equivalent diameter (D_w). The CF was derived from D_w and CF values before and after
23 miscentering correction was calculated. Finally, the CF values were compared to those calculated
24 from the axial image using the conventional methodology of the American Association of Physicists
25 in Medicine. Before miscentering correction, the maximum difference between the CF values of the
26 axial and scout images was 7.26%. However, after miscentering correction, the maximum difference
27 was 1.34%. Validation using a whole-body phantom generally revealed low maximum differences
28 between the CF from the axial image and the values from the miscentering-corrected scout images.
29 These were 2.41% in the chest, 6.30% in the upper abdomen, 1.43% in the abdomen, and 2.45% in
30 the pelvic region. Consequently, we concluded that our miscentering correction method for deriving
31 the appropriate CF values based on scout images is advantageous.

32
33 **Keywords**

34 size-specific dose estimate, computed tomography dose index, miscentering correction

35 **1. Introduction**

36 The recent popularization of multi-detector computed tomography (CT) has coincided with an
37 increase in clinical CT examinations. The radiation dose from CT is generally higher than that from
38 other diagnostic modalities; thus, it requires careful and appropriate evaluation. The volume CTDI
39 ($CTDI_{vol}$) is widely used as a radiation dose index during CT examinations and is displayed on the
40 console of CT scanners. $CTDI_{vol}$ is obtained from measurements using 16 cm and 32 cm diameter
41 and 15 cm long reference phantom; these values are often measured using an ion chamber dosimeter.
42 However, the $CTDI_{vol}$ does not account for patient size and only provides information about scanner
43 output for a very specific standardized condition [1]. Thus, the size-specific dose estimate (SSDE)
44 proposed by the American Association of Physicists in Medicine (AAPM), which permits estimates
45 based on individual patient size, has gained widespread acceptance as an alternative CT radiation
46 dose index [2-7]. SSDE is defined by the product of the $CTDI_{vol}$ and a correction factor (CF) for
47 patient size. Here, the CF is characterized by an effective diameter (D_{eff}) [2] that can be calculated
48 from the diameter of image landmarks such as lateral (LAT) projection, anteroposterior (AP)
49 projection, a combination of the two projections, or the effective area (A_{ROI}) of the patient's
50 cross-section. However, D_{eff} does not account for the attenuation of X-ray photons arising from
51 tissue density variations within the patient's body. For example, the lung is less dense than the
52 abdominal organs, and the thorax would attenuate fewer X-ray photons compared with the abdomen
53 at the same imaging parameters. To manage these variations, the water equivalent diameter (D_w) was
54 proposed to express X-ray attenuation by the patient's body in a manner equivalent to a cylindrical
55 water phantom having the same X-ray absorption; therefore, it provides accurate size-corrected dose
56 estimates [8, 9]. AAPM Report 220 proclaimed that the use of D_w is a preferred method for
57 determining the SSDE correction factors [10].

58 Conventionally, D_w and CF are determined from CT axial images. However, a fundamental
59 disadvantage of axial images is the occasional presence of truncations in the outline of the patient
60 due to the small field of view (FOV) of certain images (e.g., cardiac CT); this can make it difficult to
61 deduce the SSDE. Another disadvantage is that they cannot be obtained before scanning. Hence, to
62 avoid these problems, scout images can be used, although some drawbacks include the magnification
63 (or demagnification) of the images with respect to the patient due to miscentering, and the inability
64 to perform Hounsfield unit scale transformations. However, miscentering can be corrected using a
65 histogram of the selected slice position from the LAT scout image [11], and simple alternative scale
66 transformation methods have been proposed based on the linear relationship between pixel values
67 and the L_w value [9, 12, 13]. Nevertheless, histograms derived from scout images tend to have
68 irregular distributions depending on the CT scanner type, and the area scanned (especially the chest),
69 which leads to poor outcomes.

70 Although using scout images may have drawbacks compared to using axial images, the former is

71 appealing due to the avoidance of truncation. Moreover, if the drawbacks of using scout images are
72 appropriately addressed, more useful advantages could be attained. Scout images are taken clinically
73 to determine the position of the axial image acquisition and to activate auto exposure control (AEC),
74 which adjusts the dose according to the body thickness. Even though a certain dose quantity is
75 necessary to obtain the scout image, the patient's final radiation dose is reduced by determining the
76 minimum scanning range and activating the AEC. However, miscentering at the time of obtaining
77 the scout image incorrectly influences the tube's current adjustment by the AEC. Hence, if this
78 problem is improved, the AEC will start up correctly and result in a lowered overall radiation dose
79 for the patient [14].

80 By overcoming the drawback of miscentering through the establishment of an optimized SSDE
81 method, this study sought to harness the potential advantages of using scout images. In summary, we
82 corrected miscentering and subsequently used the digital imaging and communications in medicine
83 (DICOM) tag information to determine the optimum CF based on a miscentering-corrected CT scout
84 image. The results were compared to those based on the method proposed by the AAPM report 220,
85 and the validity of the proposed method was evaluated using a whole-body phantom.

86
87

88 **2. Materials and Methods**

89 **2.1 CT scanner and phantoms**

90 CT scans were performed on multi-detector CT systems (Aquilion ONE, Canon Medical
91 Systems, Otawara, Japan, and partly LightSpeed VCT VISION, GE Healthcare, Milwaukee, WI,
92 USA). Four cylindrical water phantoms with diameters of 6.6 cm, 19.5 cm, 25.5 cm, and 33.5 cm
93 were used to correlate pixel values of images with the water-equivalent length (L_w). The 25.5 cm
94 diameter phantom was also used to investigate the usefulness of miscentering correction. The
95 appropriate CF values for the SSDE values were determined with reference to the trunk of the
96 PBU-50 (Kyoto Kagaku) phantom (Fig. 1).



97
98

Fig. 1 The trunk of the PBU-50 (Kyoto Kagaku) phantom

99

100 2.2 Conventional CF determination via axial images

101 The AAPM's recommended SSDE method was established in 2011 as an index of radiation dose
102 on X-ray CT images. The SSDE value is expressed as a product of the previous index ($CTDI_{vol}$) and
103 CF as:

$$104 \quad SSDE = CTDI_{vol} \cdot CF. \quad (1)$$

105 The CF can be obtained by first considering the volume of the patient to be scanned as a
106 water-equivalent cylinder. The area of the circle at the axial end of that cylinder is sized to
107 encompass the tissue targeted in the axial CT image and is referred to as the water-equivalent area
108 (A_w). As shown in the AAPM report, A_w can be calculated using the mean CT number within a
109 region of interest (ROI) as:

$$110 \quad A_w = \left(\frac{\overline{CT(x,y)_{ROI}}}{1000} + 1 \right) \cdot A_{ROI}, \quad (2)$$

111 where $\overline{CT(x,y)_{ROI}}$ is the mean CT number in the ROI and A_{ROI} is the total area of the ROI ($=$
112 $\sum A_{pixel}$). D_w is the diameter of the circle comprising A_w and is thus calculated as:

$$113 \quad D_w = 2 \sqrt{\frac{A_w}{\pi}}. \quad (3)$$

114 Finally, CF can be calculated using the following equation as in AAPM report No. 220,

$$115 \quad CF = a \cdot e^{-b \cdot D_w}, \quad (4)$$

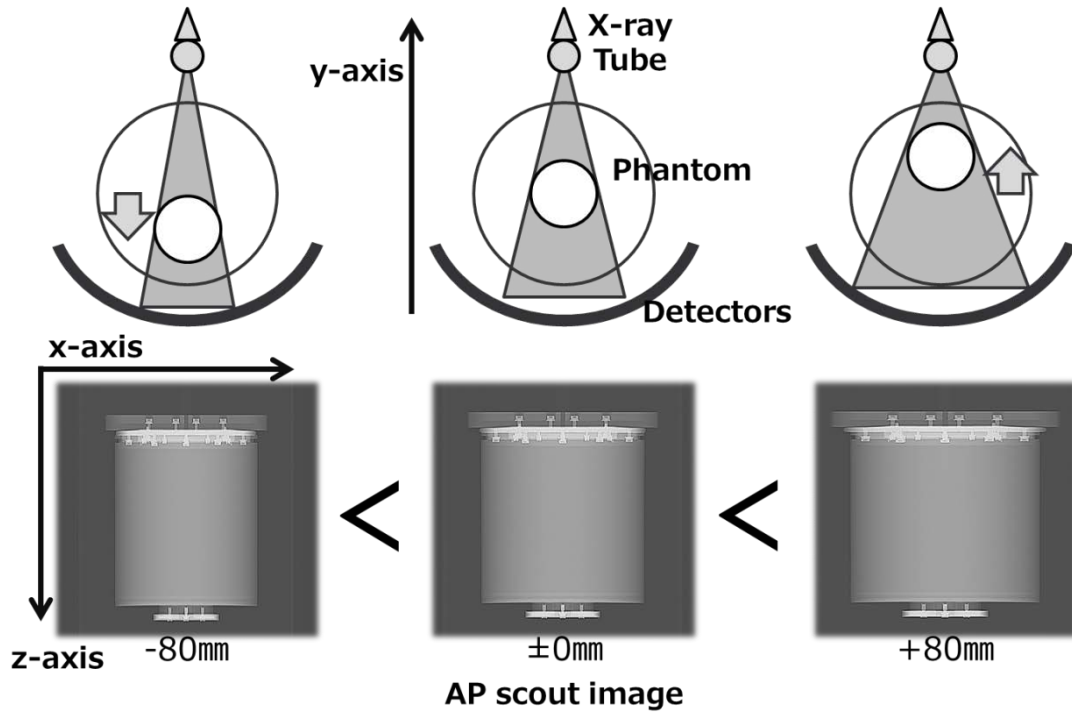
116 where $a = 3.704369$ and $b = 0.036719$. In this study, CF is based on a 32-cm-diameter CTDI
117 body phantom.

118

119 2.3 Scout image-based miscentering characteristics and correction

120 The primary limitation to the AAPM's approach using axial images is the small FOV, which can
121 truncate the patient's outline and make the A_{ROI} and SSDE difficult to establish. Scout images can be
122 used to avoid this limitation, albeit with the drawback that if the patient/phantom is miscentered
123 higher (or lower) on the y-axis than the isocenter of the CT scanner, the AP scout image is magnified
124 (or demagnified) with respect to the patient/phantom (Fig. 2).

125



126

127 **Fig. 2 Magnification or demagnification according to isocenter location. AP, anteroposterior**

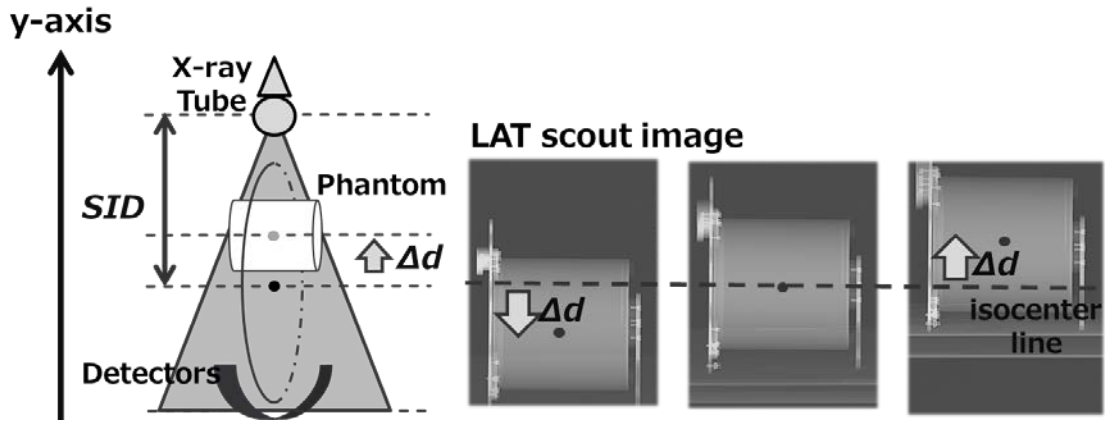
128

129 In this study, miscentering was corrected using the LAT scout image. First, we evaluated the
 130 amount of miscentering (Δd) between the phantom center and the isocenter of the CT scanner using
 131 the LAT scout image (Fig. 3). The phantom center position was defined as the midpoint between its
 132 anterior and posterior ends. The y-axis value (y-value) on the anterior side of the phantom was
 133 estimated via image thresholding. The y-value on the posterior side was set equivalent to the height
 134 of the bed displayed in the DICOM tag. The phantom center can be calculated by calculation of the
 135 difference between the anterior and posterior y-values. The y-value of the isocenter is equivalent to
 136 the center of the LAT scout image. Thus, Δd is calculated as the difference between the phantom
 137 center and the isocenter. Here, Δd is assumed to be positive in the direction of the X-ray tube and
 138 negative in the direction of the detector. Finally, the magnified (or demagnified) scout width (SW)
 139 on the AP image can be corrected to the correct width (CW) according to the following equation,
 140 which is based on the similarity rule of the object:

$$141 \quad CW = \frac{SID}{SID - \Delta d} \cdot SW. \quad (5)$$

142 Here SID stands for source-to-isodistance. SW can be obtained from the pixel width of the phantom
 143 in the AP scout image.

144



145

146

147 **Fig. 3 Miscentering (Δd) the phantom center from the isocenter on LAT scout images. LAT,**
 148 **lateral; SID, source-to-isodistance**

149

150 2.4 Pixel value and L_w in the scout image

151

152

153

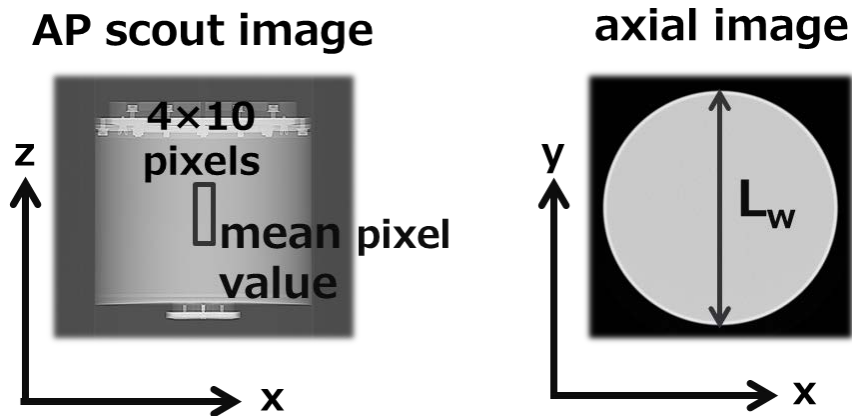
154

155

156

157

The four cylindrical phantoms were scanned in the AP and axial directions to determine the relationship between pixel value and L_w . Based on the AP scout image, the mean pixel value within a 4×10 -pixel x - z axis rectangle at the center of the phantom was determined. On the axial image, the L_w value at the center of the phantom was measured manually (Fig. 4). The results for both values are given in Table 1 for each phantom size. An excellent linear relationship between them is apparent in Figure 5.



158

159 **Fig. 4 AP and axial scout images of a cylindrical phantom, respectively, depicting the area for**
 160 **determining the mean pixel value (left) and L_w (right). AP, anteroposterior; L_w ,**
 161 **water-equivalent length**

162

163

164

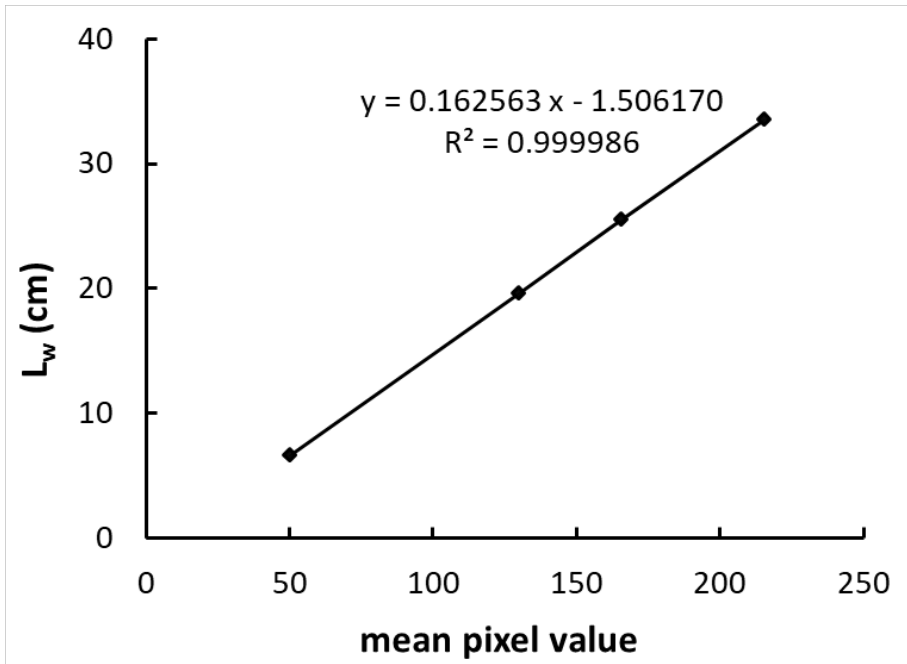
Table 1. Mean pixel value and L_w according to phantom size

phantom diameter (cm)	mean pixel value	L_w (cm)
6.6	49.93	6.62
19.5	129.73	19.53
25.5	165.63	25.47
33.5	215.50	33.52

165

166

L_w , water-equivalent length



167

168

Fig. 5 Relationship between the mean pixel value and water-equivalent length (L_w)

169

170 2.5 Scout image-based CF calculation following miscentering correction

171 The pixel value reportedly increases linearly with increasing L_w [9]. In this study, the
 172 relationship between the mean pixel value and L_w was obtained by plotting the manually derived L_w
 173 values and pixel values from Table 1 and calculating the regression line. The resulting regression
 174 equation was as follows:

175
$$L_w = 0.162563 \cdot \text{mean pixel value} - 1.506170. \quad (6)$$

176 A row of pixels from the AP scout image was selected, and their pixel values were converted to L_w
 177 using Eq. 6. Next, A_w was calculated as the product of the mean L_w ($\overline{L_w}$) for all pixels in the selected
 178 row and CW as:

179
$$A_w = \overline{L_w} \cdot CW. \quad (7)$$

180 Finally, CF values were calculated using Eqs. 3 and 4. For this study, the 25.5-cm cylindrical
 181 phantom was set at the following bed heights: -80 mm, -40 mm, 0 mm, +40 mm, and +80 mm.

182 Subsequently, the pre- and post-miscentering correction CF values were calculated for each of these
 183 bed heights. The resulting CF values were compared with the CF values that were conventionally
 184 calculated via the AAPM methodology from the axial image (2.2).

185

186 2.6 Validation of CF using a trunk part of PBU-50 phantom

187 To evaluate the validity of our scout image and miscentering correction method, a trunk phantom
 188 was scanned with its center at the isocenter of the CT scanner. Extraction of rows in the scout image
 189 was made corresponding to the slice position obtained from the DICOM header of the axial image.
 190 CF values were calculated from the axial image without any truncation at each slice position via the
 191 conventional AAPM methodology, thus permitting comparison with the scout image-based CF
 192 values calculated at the same slice positions.

193

194

195 **3. Results**

196 3.1 Evaluation of the usefulness of miscentering correction

197 The CF calculated from the axial image was 1.450. Table 2 and Figure 6 show the results for the
 198 amount of miscentering (Δd) from the LAT scout image, pre- and post-miscentering correction AP
 199 scout image CF values, the CF of the axial image, and the percent differences between the axial CF
 200 and the pre- and post-corrected AP scout image CF values. The amount of miscentering is
 201 plus-signed toward the X-ray tube and minus-signed toward the detector. Before miscentering
 202 correction, the percentage differences between the axial image CF and the AP scout image CF values
 203 ranged up to 7.26%. After miscentering correction, the maximum percentage difference in CF was
 204 reduced to 1.34% (Table 2, Figure 6). By miscentering correction, the CF value was almost constant
 205 regardless of the bed height. This trend was also confirmed for LightSpeed VCT VISION (GE
 206 Healthcare).

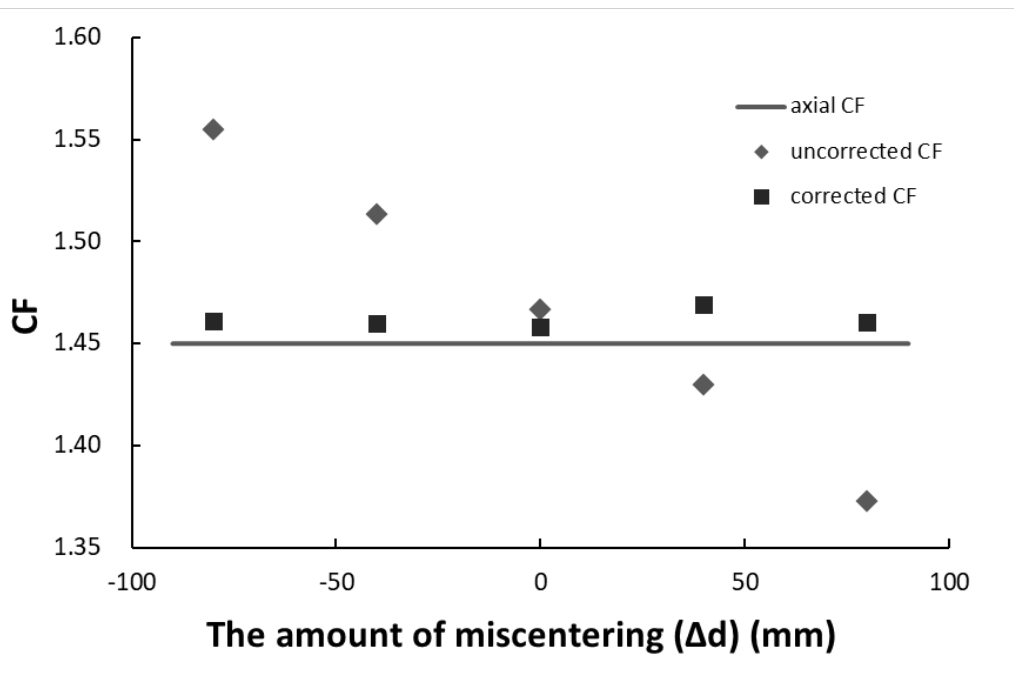
207

208 **Table 2. AP scout image CF values before and after miscentering (Δd) correction and percent**
 209 **difference from axial image CF (1.450) with Aquilion ONE**

bed height (mm)	Δd (mm)	CF before correction	difference (%)	CF after correction	difference (%)
-80	-82.520	1.555	7.264	1.461	0.758
-40	-42.480	1.513	4.380	1.460	0.693
0	-1.470	1.467	1.185	1.458	0.585
40	39.551	1.430	-1.372	1.469	1.342
80	77.637	1.373	-5.296	1.460	0.725

210

211 AP, anteroposterior; CF, correction factor



212

213

Fig. 6 Pre- and post-correction AP scout image CFs according to miscentering (Δd) amount. Δd is plus signed toward X-ray tube and minus toward detector.

214

215

216 3.2 Evaluation using a trunk phantom

217

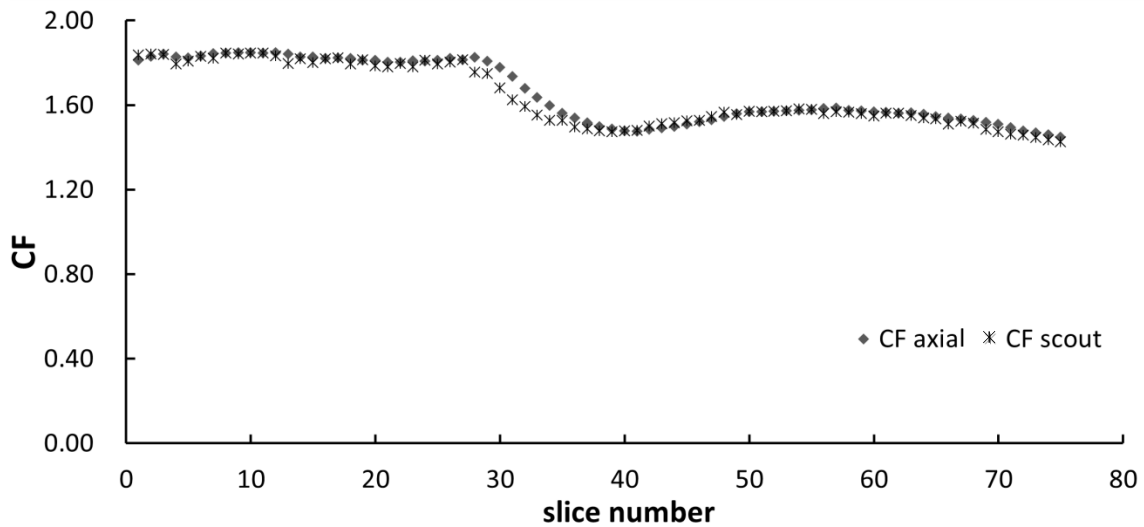
Figure 7 shows the results of the CF values from the axial image and the AP scout image at each slice position of the trunk phantom as well as the difference between them. The differences between the CF from the axial image and those from the scout images of the trunk phantom were small in all slices. The maximum differences were 2.41% in the chest, 1.43% in the abdomen, and 2.45% in the pelvic region. However, in the upper abdominal region, the maximum difference was relatively high at 6.30% (Fig. 7).

220

221

222

223



224

225 **Fig. 7 Comparison of the CF values (along the z-axis) from the axial computed tomography**
 226 **image and the AP scout image for the trunk phantom.**

227 CF, correction factor; AP, anteroposterior

228

229

230 **4. Discussion**

231 Table 2 shows that AP scout image-based miscentering can be corrected using the method
 232 proposed in this study. The anterior position of the phantom is easily or automatically extracted via
 233 processing steps such as image thresholding by using LAT scout image. However, extraction of the
 234 posterior position of the phantom is greatly influenced by the bed, which may or may not be
 235 radiographed in the scout image depending on its height. In such a case, it is difficult to extract the
 236 accurate position based on the histogram of the pixel value from the LAT scout image. It is
 237 particularly difficult to automatically extract the position of the bed in the chest region because the
 238 histograms around the chest tend to present irregular (scattering) distributions [11]. To overcome this,
 239 we established a relationship between the tag information of the bed height on the DICOM and the
 240 position coordinate in the image. Our results indicated that this relationship is linear and similar to
 241 that exhibited by another CT scanner (LightSpeed VCT VISION; GE Healthcare, Milwaukee, WI,
 242 USA). Using this relationship, we could accurately extract the posterior position of the phantom.

243 Our results clarified that magnification (or demagnification) increases as the amount of
 244 miscentering increases (Fig. 6); this finding is analogous to the result of the AAPM report 220 [10].
 245 Using our proposed method to correct this miscentering, the percentage difference between the
 246 axial-image CF and AP scout-image CF was reduced. Furthermore, the validation of our method
 247 using the trunk phantom revealed that post-correction CF values correlated with the axial image CF
 248 at almost every site, even though a slight difference appeared around the upper abdomen (slice

249 number around 30 in Fig. 7). It was unclear what caused this difference. However, AAPM task group
250 220 reports that if the difference between the pre- and post-scan (scout and axial image) values for
251 D_w and SSDE is shown to be consistently less than 10% of the pre-scan values across a range of
252 patient size and habitus, the pre-scan values can be used as the final values [10]. Thus, we concluded
253 that the use of the value from the AP scout image is fair.

254 We also calculated D_w and CF values based on the linear relationship between pixel value and
255 L_w using scout images. As previously reported, pixel value increased linearly with increasing L_w
256 [9,12]. However, because the slope and intercept of this linear function are largely dependent on the
257 type of CT scanner used, others attempting to use our method will first need to establish the
258 relationship between the pixel value and L_w for their respective CT scanners. It will also be
259 necessary to confirm the linear correlation between the tag information of the bed height on the
260 DICOM and the coordinate position of the image.

261 The miscentering correction method proposed in this study requires scanning the LAT scout
262 image and an AP scout image, a deviation from the conventional protocol. More accurate CF before
263 scanning would enable us to perform the scanning with more appropriate doses. This implies that the
264 benefits outweigh the risks of radiation in terms of radiation protection practices. However, a
265 limitation of this method is the reduced correction accuracy when the patient is decentered along the
266 LAT direction.

267 Because the trunk phantom used to validate our method is rather homogeneous in density
268 compared with the actual human body, further validation using actual clinical images is needed.

269
270

271 **5. Conclusion**

272 In this study, we proposed and validated a method to correct the problem of magnification (or
273 demagnification) that occurs due to miscentering when AP scout images are used to obtain the CF
274 for SSDE from a CT scan. Our method corrected miscentering by using an LAT scout image. Using
275 a cylindrical phantom, the maximum percentage difference between the CF values calculated
276 conventionally from an axial image and those calculated from AP scout images was reduced from
277 7.26% to 1.34% after correcting for miscentering using our method. The examination using a trunk
278 phantom revealed that the percentage differences between the CF values from an axial image and the
279 corrected AP scout images were small at almost every site, reaching a maximum of 6.30%.
280 Considering the accuracy of our method compared to that of a conventional axial image-based CF
281 calculation and the fact that scout images are less likely than axial images to be truncated, the scout
282 image-based CF calculation method may be advantageous even for clinical applications.

283
284

285

286 **Acknowledgements**

287 The authors thank Dr. Jared Boasen, Research Associate of Faculty of Health Sciences in
288 Hokkaido University, for correcting our English expressions.

289

290 **Compliance with Ethical Standards:**

291 Conflict of interest: The authors declare that they have no conflict of interest.

292 Ethical approval: The article does not contain any studies with human participants or animals
293 performed by any of the authors.

294

295 **References**

296 (1) McCollough CH, Leng S, Yu L, Cody DD, Boone JM, et al. CT Dose Index and Patient Dose:
297 They Are Not the Same Thing. *Radiology* 2011; 259:311-316.

298 (2) American Association of Physicists in Medicine. Size-specific Dose Estimates (SSDE) in
299 Pediatric and Adult Body CT Examinations. Report of AAPM Task Group 204, 2011

300 (3) Kidoh M, Utsunomiya D, Oda S, Nakamura T, et al. Breast dose reduction for chest CT by
301 modifying the scanning parameters based on the pre-scan size-specific dose estimate (SSDE). *Eur*
302 *Radiol.* 2017; 27:2267-2274

303 (4) Kawashima H, Ichikawa K, Hanaoka S, et al. Relationship between size-specific dose estimates
304 and image quality in computed tomography depending on patient size. *J Appl Clin Med Phys.* 2018;
305 19:4:246–251

306 (5) Iriuchizima A, Fukushima Y, Nakajima T, et al. Simple method of size-specific dose estimates
307 calculation from patient weight on computed tomography. *Radiation Protection Dosimetry.* 2018;
308 208-212

309 (6) Karmazyn B, Ai H, Klahr P, Ouyang F, Jennings SG. How accurate is size-specific dose estimate
310 in pediatric body CT examinations? *Pediatr Radiol.* 2016; 46:1234-1240

311 (7) Imai R, Miyazaki O, Horiuchi T, Kurosawa H, et al. Local diagnostic reference level based on
312 size-specific dose estimates: Assessment of pediatric abdominal/pelvic computed tomography at a
313 Japanese national children's hospital. *Pediatr Radiol.* 2015; 45:345–353

314 (8) Wang J, Duan X, Christner JA, Leng S, Yu L, et al. Attenuation based estimation of patient size
315 for the purpose of size specific dose estimation in CT. Part I. development and validation of methods
316 using the CT image. *Med Phys.* 2012; 39:6764-6771

317 (9) Wang J, Duan X, Christner JA, Leng S, Yu L, et al. Attenuation based estimation of patient size
318 for the purpose of size specific dose estimation in CT. Part II. Implementation on abdomen and
319 thorax phantoms using cross sectional CT images and scanned projection radiograph images. *Med*
320 *Phys.* 2012; 39:6772-6778

- 321 (10) McCollough C, Bakalyar DM, Bostani M, Brady S, et al. Use of water equivalent diameter for
322 calculating patient size and size-specific dose estimates (SSDE) in CT. Report of AAPM Task Group
323 220, 2014
- 324 (11) Li B, Behrman RH, Norbash AM. Comparison of topogram-based body size indices for CT dose
325 consideration and scan protocol optimization. *Med Phys.* 2012; 39:3456-3465
- 326 (12) Anam C, Fujibuchi T, Toyoda T, Sato N, et al. A simple method for calibrating pixel values of
327 the CT localizer radiograph for calculating water-equivalent diameter and size-specific dose estimate.
328 *Radiation Protection Dosimetry.* 2018; 179:158–168
- 329 (13) Zhang D, Mihai G, Barbaras LG, Brook OR, et al. A new method for CT dose estimation by
330 determining patient water equivalent diameter from localizer radiographs geometric transformation
331 and calibration. 2018; *Med Phys.* 2018; 45:3371-3378
- 332 (14) Koyanagi Y. The Reduction of Radiation Exposure from CT Examinations. *Japanese journal of*
333 *occupational medicine and traumatology.* 2015; 63(4):219–224